IMPLEMENTATION OF PROPORTIONAL-INTEGRAL AND PROPORTIONAL-RESONANT CONTROLLERS FOR OFF-BOARD ELECTRIC VEHICLE CHARGERS

Gyanendra Bahadur SINGH[1], Mohd. Khursheed SIDDIQUI[1], Aakash KUMAR SETH[2], Maloth NARESH[3]

In this paper, two controllers have been used to compare the off-board electric vehicle charger (EVC). Generally, two stages of conversion have been used in EV chargers, i.e., AC-DC-AC converters. The first stage controller has two loops, i.e., the inner and the outer control loop. The outer control loop is quite slow and is utilized to track the power or voltage command. The faster inner loop is used for controlling the grid current. The controlling of grid current can be done either in the dq or abc frames. In this study the dq frame has been used to control current. The regular proportional integral (PI) controller is utilized due to its capability to track the DC quantity. Whereas, in the abc frame, a proportional resonant (PR) controller has been used due to its capability to track the periodic signal of fixed frequency. Therefore, this paper presents a comparative study of current control design for the first stage of AC-DC-AC converters, focusing on both AC and DC quantities. Both PI and PR controllers have been simulated in the MATLAB/Simulink environment.

Keywords: Battery Charger, Grid to Vehicle (G2V), PEV, PI Controller, Proportional Resonant (PR) Controller, Vehicle to Grid (V2G)

1. Introduction

Electric vehicles (EVs) have gained wide acceptance worldwide in the past two decades due to the increase in carbon emission by fuel-based vehicles in the environment. As the number of EVs increases day after day, in the near future, it is projected that many EVs will link to the distribution grid [1]. This will raise the power quality issues and will cause under-voltage and over-voltage issues in the power grid. To overcome these issues, there must be a proper and smart charging system to support the grid [2]. EVs come in a variety of forms, including fuel cell EVs, PHEVs, and HVEs. [3]. The FCEVs are not significantly popular, as these vehicles suffer from hydrogen storage, fuel cell life cycle, transportation and production of hydrogen and high fuel cost [4]. In PHEVs, electricity is required

[1] Department of EEE, Integral University, Lucknow, Uttar Pradesh, India, E-mail: gbsingh933@gmail.com and khursheed20@gmail.com

[2] Department of Electrical Engineering, Government Polytechnic, Hapur, Uttar Pradesh, India, E-mail: akrseth@gmail.com

[3] Department of EEE, Guru Nanak Institute of Technology Hyderabad, Telangana, India, E-mail: naresh219.m@gmail.com

from the utility grid to charge battery banks and therefore these types of vehicles are also known as grid-able electric vehicles (GEV).

Major EVs have three parts: energy storage system (ESS) (battery, fuel cell and ultra capacitors), the PEC for battery charging and electric motor [5]. The battery bank of the EV can be charged by two ways i.e., via off or on-board charger. Where, chargers of on-board are located inside and chargers of off-board are located at the outside of the vehicle. Both the charging systems can be conductive or inductive and may be bidirectional or unidirectional. The several chargers' topologies have been presented in literature. [6]-[8]. On the basis of charging time, there are three charging levels of EVs: slow, semi-fast and fast charging [9]-[10]. Level 1 charging takes longer time (approx. overnight) to charge the battery pack. The on-board level 1 charger requires 120 or 230 V AC supply. The semi-fast method of charging is used for both private and public and needs 230 V AC supply. Whereas the fast method of charging is used for public and commercial applications and needs 208-600 V DC or three-phase AC supply.

G2V and V2G are two operating modes of an EV charger [11]-[12]. In G2V the grid supplies power to the EV for battery charging, whereas in V2G the energy available in the battery pack is transferred back to the utility grid. Moreover, an EV charger can also support the grid reactively whenever required. The reactive power supported by EV chargers can reduce the cost of compensator and capacitor banks [13]-[14]. Nevertheless, compensating for reactive power using an EV charger is not preferred, as it introduces ripple in the battery current and affects its lifecycle. [15]. Therefore, to support the grid a proper charging is required for control to track the real (P), reactive power (Q) command.

Several EV charger control strategies have previously been considered [16]-[19]. Usually, the initial step of an EV charger control architecture involves two control loops. The inner loop is intended to control grid current in the event of EV charging, the outer control loop is used to regulate active-reactive power. In comparison to the outer control loop, the inner control loop is faster. Since, PI regulators are simple in design, easy in implementation and perform well for DC quantity. Thereby, it is easier to track grid current in DC quantity by PI regulators in an inner current loop [20]. However, it requires decoupling terms in the inner loop. On the other hand, the current can be controlled after transforming it in corresponding periodic form. Since the performance of PI regulators are not satisfactory for periodic signals, it requires a controller which can track periodic signals like PR, repetitive controller (RC), etc. [21]-[22].

The PR controllers are tuned for a particular frequency, and they can be utilized to track the current in AC quantity. Therefore, this paper presents the comparative study of two inner current control designs for the first stage which are based on tracking the reference current in AC or DC quantity. In DC quantity, two PI regulators are utilized to track the corresponding DC current i.e., real (Id) and

reactive current component (Iq) with decoupling terms [23]. To track the current in AC quantity, first it transforms into an equivalent AC form then tracked by a PR controller. Moreover, the infinite gain at resonance of an ideal PR controller makes its practical implementation very challenging. Therefore, a modified PR has been designed to track the reference periodic current. In modified PR the gain and bandwidth has been adjusted at resonance frequency, so that it can be easily implemented in real time [24].

The impact of different charging techniques on off-board and on-board chargers of electric vehicles, the analysis of off-board plug-in chargers [25]-[26]. The automatic power reduction, development of wireless sensor networks for collision avoidance systems and electromechanical braking servos have been studied [27]-[29]. Both controllers have been implemented on a 6.6 KVA two-stage OFF-board EV charger in the MATLAB/Simulink environment. The charger can work under both G2V and V2G mode and performance has been investigated over the P-Q plane with all possible modes.

2. System description

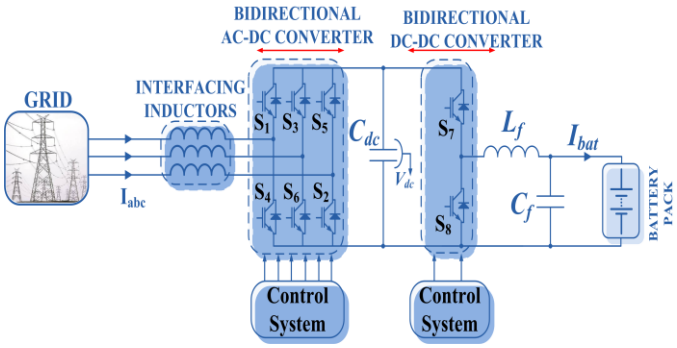

Fig. 1. EV charger

The first stage of an EV charger uses a 3-phase (3- ϕ) full bridge AC to DC converter, while the second stage uses a DC-DC buck boost converter as shown in Fig. 1. As both converters are bidirectional, the EV charger may transfer power in both directions. Both converters are built using insulated gate bipolar transistors (IGBTs) and a parallel-connected diode. The EV charger is associated to 3-ϕ grid via interfacing inductors (Ls) which are utilized to diminish the harmonics component in grid current. The DC-DC converter is attached to the battery and the DC link capacitor. Furthermore, a filter circuit is connected between the battery and DC-DC converter to minimize ripples in the voltage and current of the battery. Table I listed parameters of EV charger shown in Fig. 1. For the sake of analyzing discharging and charging behavior, the battery's starting state of charge (SOC) is assumed to be 50%. Since the voltage is dependent on SOC, the battery voltage may differ from nominal voltage.

Table 1

Charger Parameters

Parameters	Symbol	Value (Simulation)
Charger Rating	S	6.6 kVA
Grid Voltage	V_g	400 V_{LL}(rms)
Interfacing Inductor	L_s	4 mH
DC Link Capacitor	C_{dc}	1100 μF
Grid Frequency	F	50 Hz
Converter Switching Frequency	f_s	20 kHz
Battery Voltage	V_{bat}	350 V

The charger can work under maximum eight modes with different P-Q combinations [19]. When active power is positive, it signifies the charger is charging the battery and negative means it is discharging the battery. In a similar manner, positive reactive power denotes inductive operation and negative, capacitive operation.

3. Control design

For both control designs, the first stage's controller has two control loops. The charging choice (i.e. slow or fast) depends on the user, and it is directly commanded by reference active power (P_{cmd}) of the controller, whereas reference reactive power (Q_{cmd}) is requested by grid and compensated within the rating of the charger. For optimal operation, the total rating of the charger must be utilized. The maximum reactive power compensated by charger is,

$$Q_{cmd} = \sqrt{S^2 - P_{cmd}^2} \tag{1}$$

Where S is the charger's rating. First, both P and Q are designed for the AC side in the *dq* frame to regulate them in the outer loop. Moreover, phase-locked loop (PLL) is required to maintain synchronism with the utility grid. To compute P and Q, first 3-ϕ grid current (I_{abc}) and voltage (V_{abc}) are converted into *dq* using Park transformation [24].

$$\begin{bmatrix} V_{dg} \\ V_{qg} \end{bmatrix} = \frac{2}{3} * T * \begin{bmatrix} V_a \\ V_b \\ V_c \end{bmatrix} \tag{2}$$

$$\begin{bmatrix} i_{dg} \\ i_{qg} \end{bmatrix} = \frac{2}{3} * T * \begin{bmatrix} i_a \\ i_b \\ i_c \end{bmatrix} \tag{3}$$

Where,

$$T = \begin{bmatrix} \cos(\omega t) & \cos\left(\omega t - \frac{2\pi}{3}\right) & \cos\left(\omega t - \frac{4\pi}{3}\right) \\ \sin(\omega t) & \sin\left(\omega t - \frac{2\pi}{3}\right) & \sin\left(\omega t - \frac{4\pi}{3}\right) \end{bmatrix} \quad (4)$$

The P and Q can be computed by using *dq* component of grid voltage and current as follows:

$$P = 1.5(V_{dg}.i_{dg} + V_{qg}.i_{qg}) \quad (5)$$

$$Q = 1.5(V_{dg}.i_{dg} - V_{qg}.i_{qg}) \quad (6)$$

This measured P and Q contains the DC as well as oscillating terms, therefore a LPF is utilized to calculate the average value.

PI controllers are instructed to real (P_{cmd}) and reactive (Q_{cmd}) power, respectively, and produce the references for the active (i_{dg}^{*}) and reactive (i_{qg}^{*}) current components, as follows:

$$i_{dg}^{*} = K_{p1}(P_{cmd} - P) + \frac{K_{i1}}{s}(P_{cmd} - P) \quad (7)$$

$$i_{qg}^{*} = K_{p2}(Q_{cmd} - Q) + \frac{K_{i2}}{s}(Q_{cmd} - Q) \quad (8)$$

Where K_{p1} and K_{i1} are the PI controller's proportional and integral constants for controlling active power, while K_{p2} and K_{i2} are the same for controlling reactive power. The P_{cmd} is the reference of charging/discharging rate for EV battery packs, and Q_{cmd} is the reference of reactive power compensation demanded by the utility grid.

A. In dq Frame

Fig. 2 shows the EV charger controller where grid current is controlled in the *dq* frame in an inner loop.

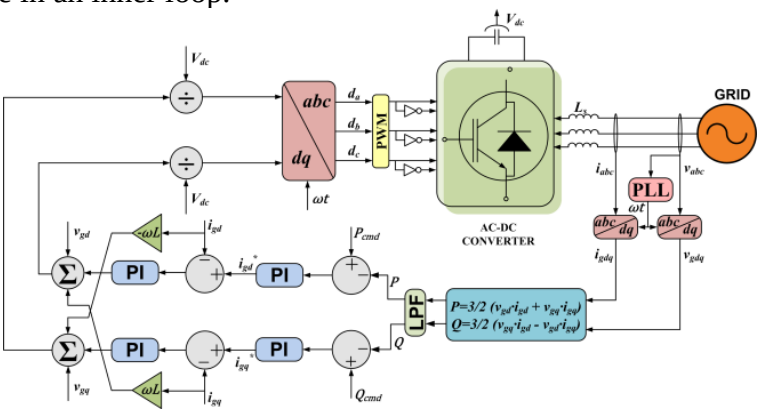

Fig. 2. System Control using inner current control in *dq* frame.

The inner loop is developed by comparing *dq* reference current with *dq* component of actual current. The active and reactive current *PI* regulators generate the e_d and e_q, respectively.

$$e_d = K_{p3}(i_d^* - i_d) + \frac{K_{i3}}{s}(i_d^* - i_d) \tag{9}$$

$$e_q = K_{p4}(i_q^* - i_q) + \frac{K_{i4}}{s}(i_q^* - i_q) \tag{10}$$

Where, K_{p3} and K_{p4} & K_{i3} and K_{i4} are PI constants to control the P & Q power. The DC link voltage to create duty cycles in the *dq* frame.

$$\begin{bmatrix} d_d \\ d_q \end{bmatrix} = \frac{1}{V_{dc}} \begin{bmatrix} e_d + v_d + 3\omega L * i_q \\ e_q + v_q + 3\omega L * i_d \end{bmatrix} \tag{11}$$

Furthermore, these duty cycles are converted into corresponding *abc* frames by using inverse transformation and pulses are produced through pulse width modulation (PWM) technique.

$$\begin{bmatrix} D_a \\ D_b \\ D_c \end{bmatrix} = T^T \begin{bmatrix} d_d \\ d_q \end{bmatrix} \tag{12}$$

Where,

$$T^T = \begin{bmatrix} \cos(\omega t) & \sin(\omega t) \\ \cos\left(\cos(\omega t - \frac{2\pi}{3}\right) & \sin\left(\cos(\omega t - \frac{2\pi}{3}\right) \\ \cos\left(\cos(\omega t - \frac{4\pi}{3}\right) & \sin\left(\cos(\omega t - \frac{4\pi}{3}\right) \end{bmatrix} \tag{13}$$

B. In the abc Frame

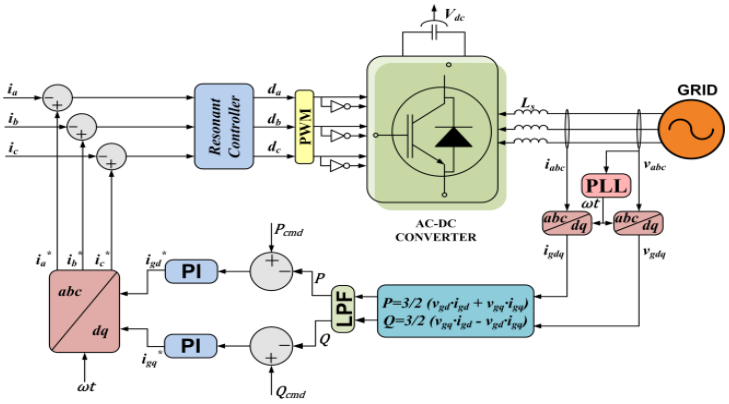

Fig. 3. System Control using inner current control in abc frame.

Fig. 3 shows the EV charger controller where grid current is regulated in the *abc* frame. Here, the component of current is transformed into the corresponding *abc* frame.

$$\begin{bmatrix} i_a^* \\ i_b^* \\ i_c^* \end{bmatrix} = T^T \begin{bmatrix} i_{dg}^* \\ i_{qg}^* \end{bmatrix} \tag{14}$$

Now, the 3-ϕ grid current is compared to these reference currents, and the error is reduced by utilizing a PR controller.

$$\begin{bmatrix} e_a \\ e_b \\ e_c \end{bmatrix} = \begin{bmatrix} i_a^* - i_a \\ i_b^* - i_b \\ i_c^* - i_c \end{bmatrix} \tag{15}$$

Where, e_a, e_b and e_c are errors in current with corresponding phase, respectively.
The PR controllers generate the duty cycles in *abc* frames and pulses are generated by using PWM techniques.

$$\begin{bmatrix} D_a \\ D_b \\ D_c \end{bmatrix} = \begin{bmatrix} K_{pa}.e_a + \left(K_{Ra} \dfrac{2\omega_c S}{S^2 + 2\omega_c S + \omega^2} \right).e_a \\ K_{pb}.e_b + \left(K_{Rb} \dfrac{2\omega_c S}{S^2 + 2\omega_c S + \omega^2} \right).e_b \\ K_{pc}.e_c + \left(K_{Rc} \dfrac{2\omega_c S}{S^2 + 2\omega_c S + \omega^2} \right).e_c \end{bmatrix} \tag{16}$$

Where, K_{pa}, K_{pb} and K_{pc} are proportional and K_{Ra}, K_{Rb} and K_{Rc} are resonant constants of the PR controller, respectively.

The term $\left\{ K_p + \dfrac{2K_R\omega_c S}{S^2 + 2\omega_c S + \omega^2} \right\}$ is PR controller transfer function. The ideal PR controller is difficult to implement practically and has infinite gain at resonance frequency. Therefore, the gain must be restricted to a certain finite value, and it is done by adding cut off frequency (ωc) in the denominator of the ideal PR transfer function. This will result in an increment of bandwidth and also at resonance frequency. The gain margin, phase margin and transient response are calculated by the value of proportional gain (Kp). Whereas the resonant gain (KR) is also responsible to limit the magnitude at resonance frequency [19].

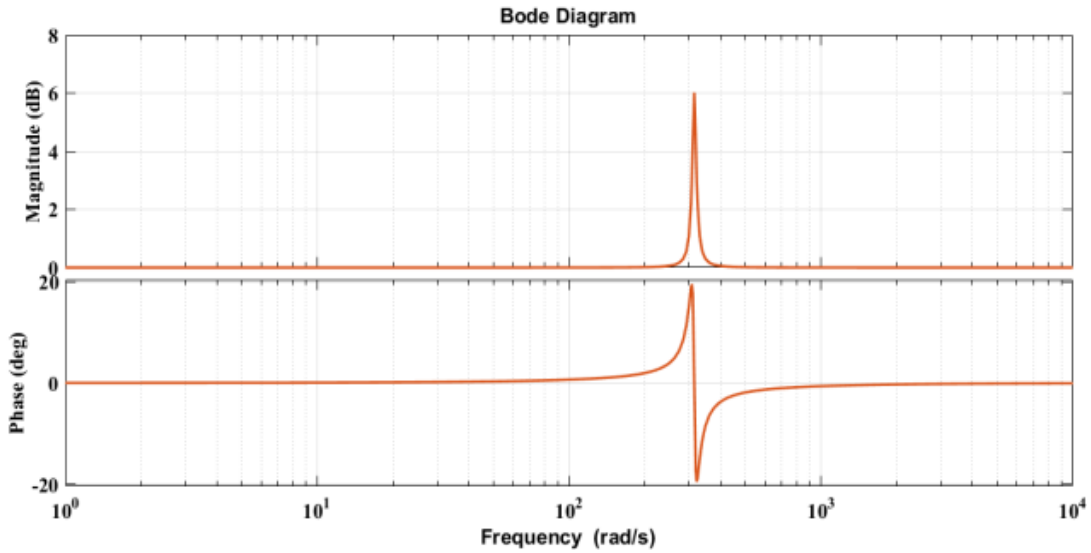

Fig. 4. Frequency response of practical PR controller.

The practical PR controller's frequency response is shown in Fig. 4. At resonance frequency, the frequency response of an ideal PR has infinite gain and an extremely small bandwidth. Here, the gain is limited up to 6 dB and bandwidth is increased by modifying the transfer function of ideal PR.

C. ***DC-DC Converter Control***

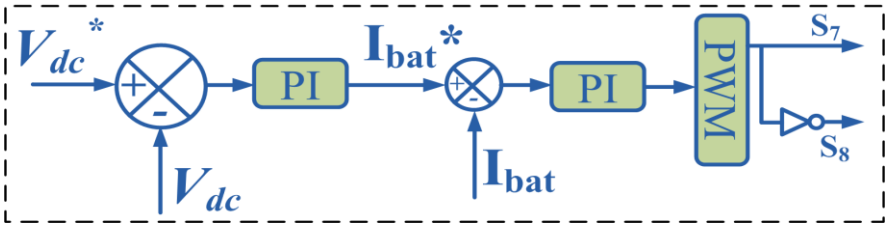

Fig. 5. DC-DC converter control.

Fig. 5 depicts the second stage's DC-DC converter's control design. Here, a second stage converter controller regulates the battery current (I_{bat}) and DC link voltage (V_{dc}). The reference and real DC link voltages are compared, and the PI controller minimizes error. This DC link voltage regulator generates the battery current reference. Further, the PI regulator, which creates the duty ratio for the DC-DC converter, regulates the battery current in the inner loop.

$$I_{bat}^{*} = K_{p5}\left(V_{dc}^{*} - V_{dc}\right) + \frac{K_{i5}}{S}\left(V_{dc}^{*} - V_{dc}\right) \tag{17}$$

$$d = K_{p6}\left(I_{bat}^{*} - I_{bat}\right) + \frac{K_{i6}}{S}\left(I_{bat}^{*} - I_{bat}\right) \tag{18}$$

4. Simulation results and discussion

Table 2

Simulation Scenario

Mode	Active Power (kW)	Reactive Power (kVAR)	Charger Rating (kVA)	Time (sec)
1	6.6	0	6.6	0-1.5
2	-6.6	0	6.6	1.5-3
3	0	6.6	6.6	3-4.5
4	0	-6.6	6.6	4.5-6
5	5.28	3.96	6.6	6-7.5
6	3.96	-5.28	6.6	7.5-9
7	-2.904	5.93	6.6	9-10.5
8	-5.93	-2.904	6.6	10.5-12

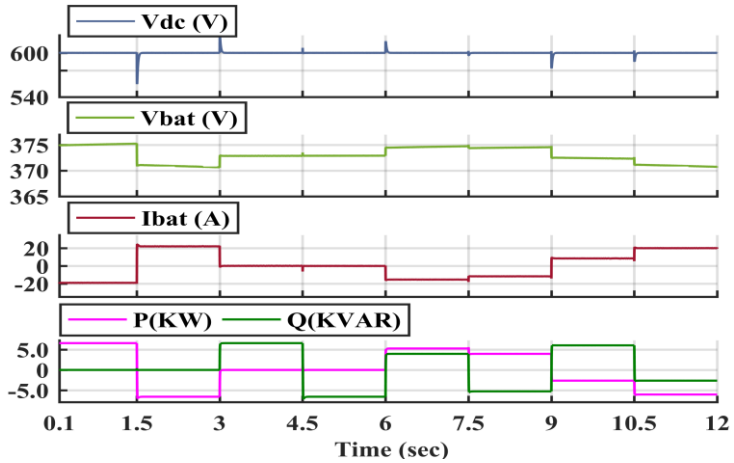

Fig. 6. *P and Q* power, battery voltage (V_{bat}), battery current (I_{bat}) and DC link voltage (V_{dc}).

MATLAB/Simulink environment is utilized to simulate both the controls for a 6.6 kVA two stage off-board EV charger. To verify the controllers' transient and steady-state responses, a simulation scenario (shown in Table 2) with various P and Q values has been created. In table 1, the system parameters are listed. Here, in the first four modes the charger is commanded to perform a single operation only (either charge/discharge or inductive/capacitive reactive power compensation). In rest four modes, the charger is commanded to perform both operations simultaneously i.e., active and reactive.

The simulation results of DC-link voltage (V_{dc}), battery voltage (V_{bat}), current (I_{bat}) and P & Q during all the modes are presented in Fig. 6. Battery voltage is seen to be consistent across all working modes, however battery current varies in accordance with the charge/discharge rate, which is positive while discharging and negative when charging. The DC-link is regulated at 600 V in all working modes.

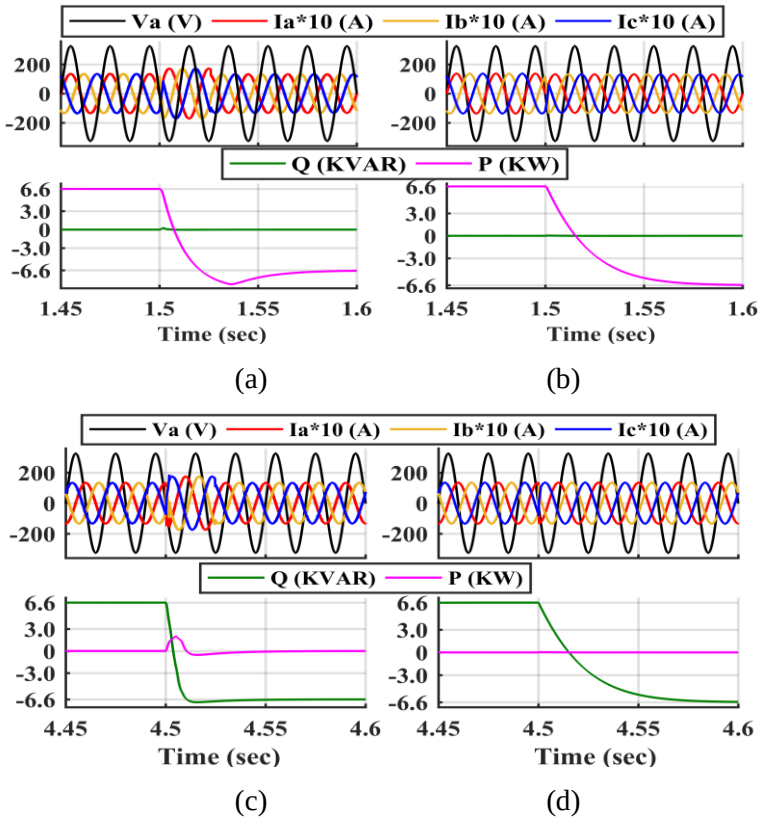

Fig. 7. Transition in *dq* frame from (a) mode 1-2, (c) mode 3-4, and in *abc* frame (b) mode 1-2, (d) mode 3-4.

The transitions of P, Q, grid voltage (V_a) and current (I_a, I_b and I_c) from one mode to another are shown in Fig. 7 and 8. Where, V_a is the phase to ground voltage of phase *a*. EV battery is charging in Mode 1, while mode 2 demonstrates the discharging operation. During charging, the phase variance between phase *a* current and voltage is zero and 180° in discharging operation. Fig. 7 (a) and (b) show the zoomed versions transition from the mode 1 to mode 2 in the *dq* and *abc* frames, respectively. Similarly, Fig. 7 (c) and (d) show the changeover from mode 3 to 4 in the *dq* and *abc* frames, respectively. During this, the phase voltage and current are displaced by 90° from each other (i.e., lagging for inductive and leading for capacitive operation). Fig. 8 (a) and (b) depict the change from mode 5 to 6 in the *dq* and *abc* frames respectively. Both the operations are related to compensation of reactive power and charging. In mode 5, the battery charges at 5.2 kW and 3.96 kVAR, and in mode 6 the process is reversed. During mode 5 and 6, the phase difference between current and voltage is around 36° and 53°, respectively.

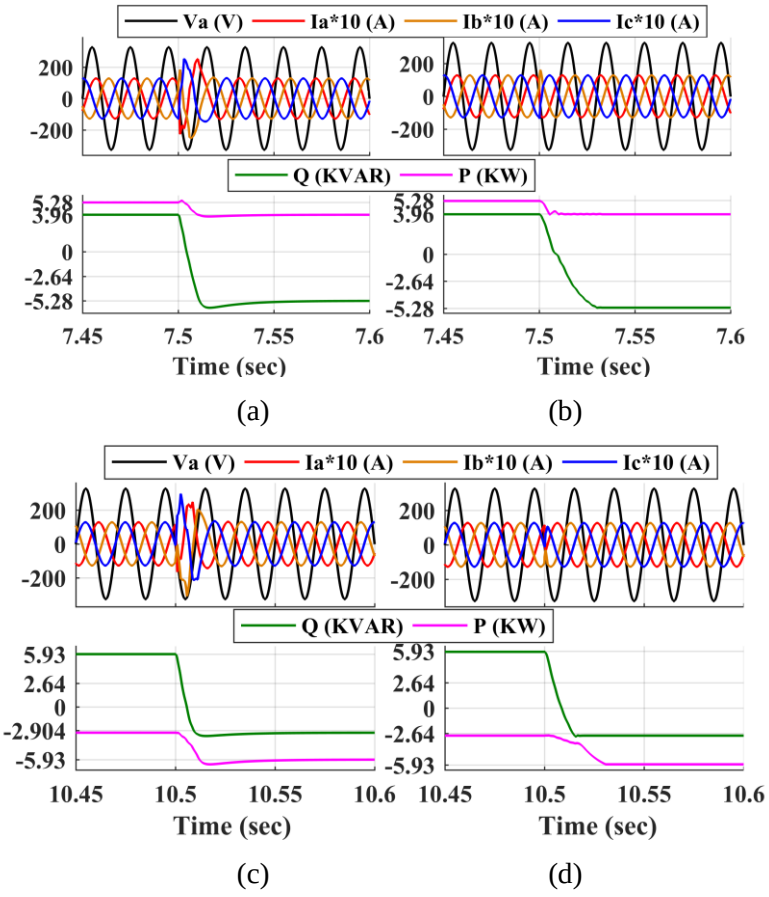

Fig. 8. Transition in *dq* frame from (a) mode 5-6, (c) mode 7-8 and in *abc* frame (b) mode 5-6, (d) mode 7-8.

Similarly, while transacting from mode 7 to 8, the phase difference is 116° and 206° in mode 7 and 8, respectively. The zoomed versions of transitions between these modes in *dq* and *abc* frames are shown in Fig. 8 (c) and (d) respectively.

It can be observed from simulation results, that in the *dq* frame a current spike occurs at the time of transition and overshoot also arises in measured active and reactive power. Nevertheless, the grid current settles faster in the *abc* frame without any spikes and overshoot in active-reactive power. Furthermore, the settling time of the output power loop is almost the same in both control algorithms and takes less than 0.06 seconds to settle down.

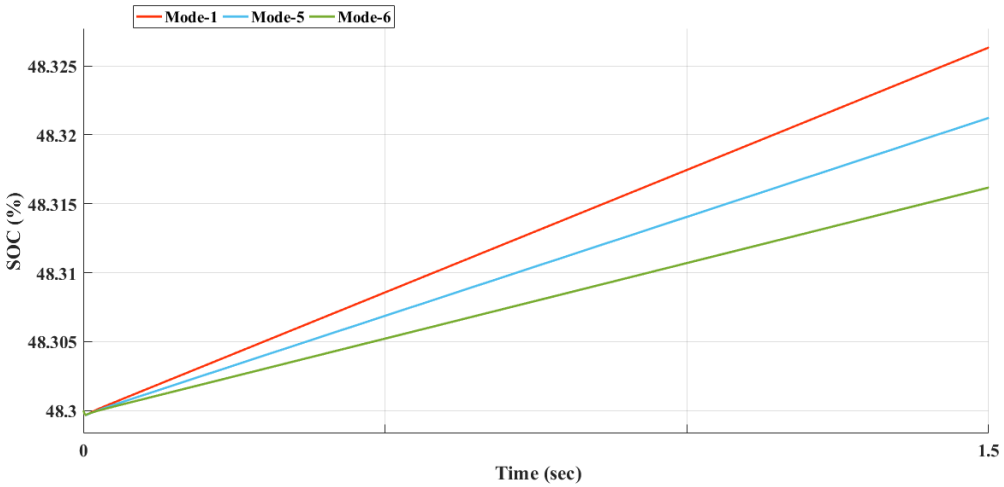

Fig. 9. SOC during mode 1, 5 and 6.

Fig. 9 depicts the variation of SOC with different charging modes. With an increase in active power supply, the SOC rises. The battery charges faster in mode 1 as 6.6 KW is transferred to the battery. However, in mode 6, it moves slowly as the amount of real power is less i.e., 3.96 KW. Moreover, the *PR* regulator suffers from frequency variations and its performance may degrade in that case and the settling time and overshoot comparison is shown in Table 3.

Table 3:

Comparison of PI and PR controller

#	PI Controller	PR controller
Settling Time (sec)	0.015	0.005
Overshoot	200%	128%

5. Conclusion

In this article two controllers have been compared for an OFF grid-EV charger. The MATLAB/Simulink environment is used to simulate the control architectures. The first controller, which controls the grid current in the *dq* frame, is based on *PI* regulators. The second control algorithm uses a *PR* regulator, in this grid current transformed in an *abc* frame before controlling it. The performance of both controllers is tested in eight different modes in the *P-Q* plane. It has been observed that the controller having *PI* regulators experienced overshot in measured *P* and *Q* and spikes in grid current. Further, tuning four *PI* regulators for a single control architecture is exceedingly difficult. However, while controlling the grid current using the *PR* controller gives satisfactory performance without any overshoot and current spikes. It has been observed that,

compared to the *PI* controller, the *PR* controller provides better performance in both steady-state and transient analysis.

REFERENCES

[1] A. K. Seth and M. Singh, “Plant integrated proportional integrating based control design for electric vehicle charger,” Computers and Electrical Engineering, vol. 105, Jan 2023.

[2] S. S. Williamson, A. K. Rathore and F. Musavi, "Industrial Electronics for Electric Transportation: Current State-of-the-Art and Future Challenges," in IEEE Transactions on Industrial Electronics, vol. 62, no. 5, pp. 3021-3032, May 2015.

[3] A. Emadi, Y. J. Lee and K. Rajashekara, "Power Electronics and Motor Drives in Electric, Hybrid Electric, and Plug-In Hybrid Electric Vehicles," in IEEE Transactions on Industrial Electronics, vol. 55, no. 6, pp. 2237-2245, June 2008.

[4] Ronald Jurgen, "Fuel-Cell Hybrid EVs," in Electric and Hybric-Electric Vehicles: Fuel Cell Hybrid EVs, SAE, pp.9-9, 2011.

[5] A. Choudhary, S. Fatima and B. K. Panigrahi, "State of the Art Technologies in Fault Diagnosis of Electric Vehicles: A Component-Based Review," in IEEE Transactions on Transportation Electrification, 2022, doi: 10.1109/TTE.2022.3209166.

[6] P. Asthana and V. Verma, "PV Fed Current Controlled Low Stress High Gain Converter for Battery Charging Applications," 2020 IEEE International Conference on Power Electronics, Smart Grid and Renewable Energy (PESGRE2020), Cochin, India, 2020, pp. 1-4.

[7] M. Yilmaz and P. T. Krein, "Review of Battery Charger Topologies, Charging Power Levels, and Infrastructure for Plug-In Electric and Hybrid Vehicles," in IEEE Transactions on Power Electronics, vol. 28, no. 5, pp. 2151-2169, May 2013.

[8] K. Fahem, D. E. Chariag and L. Sbita, "On-board bidirectional battery chargers topologies for plug-in hybrid electric vehicles," 2017 International Conference on Green Energy Conversion Systems (GECS), Hammamet, Tunisia, 2017, pp. 1-6, doi: 10.1109/GECS.2017.8066189.

[9] S. Chalia, A. K. Seth and M. Singh, “Electric Vehicle Charging Standards in India and Safety Consideration,” IEEE 8th Uttar Pradesh Section International Conference on Electrical, Electronics and Computer Engineering (UPCON), pp. 1-6, 2021.

[10] T. Anegawa, “Development of quick charging system for electric vehicle,” in Proc. World Energy Congress, 2010.

[11] A. K. Seth and M. Singh, “Unified adaptive neuro-fuzzy inference system control for OFF board electric vehicle charger,” International Journal of Electrical Power & Energy Systems, vol. 130, Sep 2021.

[12] S. Mittal, A. Singh and P. Chittora, "EV Control in G2V and V2G modes using SOGI Controller," 2022 IEEE 3rd Global Conference for Advancement in Technology (GCAT), Bangalore, India, 2022, pp. 1-6, doi: 10.1109/GCAT55367.2022.9972182.

[13] M. Restrepo, J. Morris, M. Kazerani and C. A. Cañizares, "Modeling and Testing of a Bidirectional Smart Charger for Distribution System EV Integration," in IEEE Transactions on Smart Grid, vol. 9, no. 1, pp. 152-162, Jan. 2018.

[14] M. C. Kisacikoglu, B. Ozpineci and L. M. Tolbert, "EV/PHEV Bidirectional Charger Assessment for V2G Reactive Power Operation," in IEEE Transactions on Power Electronics, vol. 28, no. 12, pp. 5717-5727, Dec. 2013.

[15] A. K. Seth and M. Singh, "Second-Order Ripple Minimization in Single-Phase Single-Stage Onboard PEV Charger," in IEEE Transactions on Transportation Electrification, vol. 7, no. 3, pp. 1186-1195, Sept. 2021, doi: 10.1109/TTE.2021.3049559.

[16] D. B. Wickramasinghe Abeywardana, P. Acuna, B. Hredzak, R. P. Aguilera and V. G. Agelidis, "Single-Phase Boost Inverter-Based Electric Vehicle Charger With Integrated Vehicle to Grid Reactive Power Compensation," in IEEE Transactions on Power Electronics, vol. 33, no. 4, pp. 3462-3471, April 2018.

[17] M. Restrepo, J. Morris, M. Kazerani and C. A. Cañizares, "Modeling and Testing of a Bidirectional Smart Charger for Distribution System EV Integration," in IEEE Transactions on Smart Grid, vol. 9, no. 1, pp. 152-162, Jan. 2018.

[18] T. He, J. Zhu, D. D. Lu and L. Zheng, "Modified Model Predictive Control for Bidirectional Four-Quadrant EV Chargers with Extended Set of Voltage Vectors," in IEEE Journal of Emerging and Selected Topics in Power Electronics, vol. 7, no. 1, pp. 274-281, March 2019.

[19] A. K. Seth and M. Singh, "Resonant controller of single-stage off-board EV charger in G2V and V2G modes," in IET Power Electronics, vol. 13, no. 5, pp. 1086-1092, 8-4-2020.

[20] M. Kesler, M. C. Kisacikoglu and L. M. Tolbert, "Vehicle-to-Grid Reactive Power Operation Using Plug-In Electric Vehicle Bidirectional Offboard Charger," in IEEE Transactions on Industrial Electronics, vol. 61, no. 12, pp. 6778-6784, Dec. 2014.

[21] G. Pandove, A. Trivedi, and M. Singh, "Repetitive control-based single-phase bidirectional rectifier with enhanced performance," IET Trans. Power Electronics., vol. 9, no.5, pp. 1029-1036, Apr. 2016.

[22] A. Trivedi, and M. Singh, "Repetitive Controller for VSIs in Droop Based AC-Microgrid," IEEE Trans. Power Electronics, Vol. 32, No. 8, pp. 6595-6604, Aug.-2017.

[23] Teodorescu, Remus, Frede Blaabjerg, Marco Liserre and Poh Chiang Loh. "Proportional-resonant controllers and filters for grid-connected voltage-source converters." IEE Proceedings, The Institution of Engineering and Technology (2006).

[24] Yazdani, A., Iravani, R.: 'Voltage-sourced converters in power systems: modeling, control, and applications' (Wiley-IEEE Press, USA, 2010).

[25] D. Kumar, S. Saha and M. Das, "Effect of Various Charging Methods on Off-Board and On-Board Chargers of Electric Vehicles," 2023 IEEE International Conference on Power Electronics, Smart Grid, and Renewable Energy (PESGRE), Trivandrum, India, 2023, pp. 1-6.

[26] T. Bazaz, A. A. Dar and F. I. Bakhsh, "Modelling and Analysis of an Off-board Plug-in Charger for Electric Vehicles," 2023 IEEE 20th India Council International Conference (INDICON), Hyderabad, India, 2023, pp. 898-903

[27] Andrei Stan, Florin Emilian Ciaușiu, Andrei Pupăză "Automatic Power Reduction Concept for Renewable Generation Sites" Journal of Scientific Bulletin Electrical Engineering and Computer Science U.P.B. Sci. Bull., Series C, Vol. 85, Iss. 4, 2023

[28] P Parthasarathy, K S Chandragupta Mauryan, and Maloth Naresh, "Development of Wireless Sensor Network for Collision Avoidance System Using Emergency Situation Prediction Mechanism" Journal of Scientific Bulletin Electrical Engineering and Computer Science, U.P.B. Sci. Bull., Series C, Vol. 85, Iss. 2, 2023.

[29] Andrei-Constantin Rădulescu-Gămaleț, Octavian Nica, Constantin Călinoiu, Nicolae Vasiliu "Electromechanical braking servos for electric vehicles - simulations and experimental validation", Journal of Scientific Bulletin Electrical Engineering and Computer Science U.P.B. Sci. Bull., Series C, Vol. 85, Iss. 3, 2023